The Cryosphere, 7, 217–227, 2013
www.the-cryosphere.net/7/217/2013/
doi:10.5194/tc-7-217-2013

The Cryosphere Open Access

Thermal conductivity of snow measured by three independent methods and anisotropy considerations

F. Riche and M. Schneebeli

WSL Institute for Snow and Avalanche Research SLF, Davos Dorf, Switzerland

Correspondence to: M. Schneebeli (schneebeli@slf.ch)

Received: 4 April 2012 – Published in The Cryosphere Discuss.: 25 May 2012
Revised: 20 December 2012 – Accepted: 4 January 2013 – Published: 6 February 2013

Abstract. The thermal conductivity of snow determines the temperature gradient, and by this, it has a direct effect on the rate of snow metamorphism. It is therefore a key property of snow. However, thermal conductivities measured with the transient needle probe and the steady-state, heat flux plate differ. In addition, the anisotropy of thermal conductivity plays an important role in the accuracy of thermal conductivity measurements. In this study, we investigated three independent methods to measure snow thermal conductivity and its anisotropy: a needle probe with a long heating time, a guarded heat flux plate, and direct numerical simulation at the microstructural level of the pore and ice structure. The three methods were applied to identical snow samples. We analyzed the consistency and the difference between these methods. As already shown in former studies, we observed a distinct difference between the anisotropy of thermal conductivity in small rounded grains and in depth hoar. Indeed, the anisotropy between vertical and horizontal thermal conductivity components ranges between 0.5–2. This can cause a difference in thermal conductivity measurements carried out with needle probes of up to −25 % to +25 % if the thermal conductivity is calculated only from a horizontally inserted needle probe. Based on our measurements and the comparison of the three methods studied here, the direct numerical simulation is the most reliable method, as the tensorial components of the thermal conductivity can be calculated and the corresponding microstructure is precisely known.

1 Introduction

Thermal conductivity is an important physical property of snow. It is especially important to understand heat transfer and mass flux in snow, since snow has a significant effect on the large scale heat budget of the Earth surface. It is a very relevant factor to the Earth's climate system as heat flows through the snow on the ground (Cook et al., 2007). Given a heat flux, thermal conductivity determines the temperature gradient through the snow pack and it is therefore one of the most fundamental properties determining the rate of snow metamorphism. It is therefore not surprising that the first measurements of thermal conductivity of snow were conducted in the late 19th century (for an overview see Sturm et al., 1997). However, science is still struggling to find the most reliable methods to measure effective thermal conductivity, k_{eff} in snow, and, in a next step, to establish a correlation between microstructure and measurements (Calonne et al., 2011). Recent interest in these questions has increased due to the inconsistencies between measurements, their regression curves and simulation models (e.g. between Sturm et al., 1997 and Calonne et al., 2011).

The reason why the measurement of thermal conductivity in snow is difficult is multifaceted. First, snow measurement methods are not standardized, and only recently Calonne et al. (2011) have compared some measurements with different instruments on the same snow samples. This is a serious shortcoming, as it is very difficult (even impossible) to find exactly the same snow structure twice. The often limited number of measurements makes the parameters of the fitting curves difficult to compare. Second, snow is in many cases extremely fragile, causing artifacts during extraction of the sample or during measurement. For this reason usually

only one or very few measurements are made within the same snow sample and therefore the intersample variability is not well determined. Third, the microstructural characterization of snow was for a long time semi-quantitative. The recent advent of microtomography and stereological techniques allows for a much more precise quantification beyond porosity. These techniques provide, for example, specific surface area and thickness distributions of ice and air.

Thermal conductivity is important in many different domains, such as food science (Nesvadba, 1982; Cogne, 2003), soil science (Vonherzen and Maxwell, 1959; Abu-Hamdeh and Reeder, 2000) and Earth science (Brigaud and Vasseur, 1989; Popov et al., 1999). In all these areas similar problems in snow are apparent; especially important is the contact problem when measuring with needle probes (Riche and Schneebeli, 2010a).

Measurement techniques of thermal conductivity fall in three main classes: steady-state methods, transient methods, and direct numerical simulations. The steady-state method uses the heat flux plate.The heat flux plate measures the heat flux through two plates placed at each side of the measured sample. The method is standardized in ASTM (2008). This method was used e.g. by Izumi and Huzioka (1975) and Yamada et al. (1974). Needle probe instruments are based on the transient line heat source method (De Vries, 1952; Blackwell, 1954). They are widely used in snow science (Lange, 1985; Sturm and Johnson, 1992; Morin et al., 2010). A variant of these two methods that is applicable to smooth surfaces, is the divided bar method generally used to measure the thermal conductivity of rocks and sediments (Pribnow et al., 2000). The Fourier method, as it was first used by Abels (1892) and recently by Brandt and Warren (1997), measures the approximately sinusoidal temperature change in the ground, and gives a thermal conductivity averaged over the depth of the temperature sensor. During the past decade, the direct numerical simulation of the thermal conductivity was developed (Ams et al., 2001; Kaempfer et al., 2005; Petrasch et al., 2008; Calonne et al., 2011). This computational method has the advantage that the 3-D microstructure is known. Together with the well-known thermal conductivity of ice and air, the effective thermal conductivity of the snow can be calculated.

A problem which has received relatively little attention is the thermal anisotropy in snow. Izumi and Huzioka (1975) made a detailed study on the anisotropy of the snow thermal conductivity, and its evolution during temperature gradient metamorphism. More recently, some studies pointed out the thermal anisotropy of snow (Calonne et al., 2011; Shertzer and Adams, 2011). The determination of anisotropy is an important part of this study.

The thermal conductivity of porous media can be anisotropic. In this case, the effective thermal conductivity k_{eff} is a tensor (Incropera et al., 2006) (in the following, we write for simplicity of notation: k instead of k_{eff}) with $-\boldsymbol{j} = k\nabla\boldsymbol{T}$, where $\boldsymbol{j}$ is the heat flux in x, y, z, k is the thermal conductivity tensor with the diagonal components k_{x}, k_{y}, k_{z} (orthorhombic system) and $\nabla\boldsymbol{T}$ is the temperature gradient in x, y, z in a Cartesian coordinate system. In the following, we assume $k_{\mathrm{x}} = k_{\mathrm{y}}$, because a snowpack usually has a horizontal layering. Arons and Colbeck (1995) refer to Izumi and Huzioka (1975) for measurements of anisotropy. However, there are in fact very few experiments measuring tensorial components. Riche and Schneebeli (2010b) measured two components (horizontal k_{x} and vertical k_{z}), assuming $k_{\mathrm{x}} = k_{\mathrm{y}}$, with the same computer simulation as used in the present study. Calonne et al. (2011) computed all tensorial components of thermal conductivity.

The determination of thermal conductivity is simplified in almost all regression equations (for an overview see Armstrong and Brun, 2008) to 1-D form, and $k = k_{\mathrm{z}}$, with k_{z} being the vertical component. If heat flow is measured parallel to the bedding of the snowpack, and the isotherm at the top and the bottom are parallel, then heat flow will be perpendicular to the bedding, independent of an anisotropic structure. Therefore, anisotropy is irrelevant if regression equations of thermal conductivity are used under such conditions. However, as we show in this paper, this bias was not always corrected for all instruments, especially in the case of the needle probe. The theory for this case will be introduced in Sect. 2.2.2.

Heat flux in snow is not purely conductive: it has also a latent heat component. Latent heat is generated through the phase change induced by recrystallization (Pinzer and Schneebeli, 2009b). The ratio between conductive heat flux and latent heat flux depends on the absolute temperature and the temperature gradient. We address this phenomenon in Sect. 2.2.4.

We focus on three fundamentally different methods to measure the thermal conductivity of snow: guarded heat flux plate (HFP), single needle probe (NP) and direct numerical simulation (SIM). The main objective is to understand the accuracy and the limitations of these three methods with consideration of thermal anisotropy. To compare the methods, the same snow samples were used for each method, although each method has a different characteristic measurement volume. We analyzed the effect of thermal anisotropy of snow on NP measurements and the effect of latent heat flux in HFP measurements. We corrected the effective thermal conductivity measured with the NP, $k_{\mathrm{eff}}^{\mathrm{NP}}$ for anisotropy. To exclude effects specific to snow, we compared HFP and NP with inert materials. These materials were chosen to cover the range of thermal conductivity typical for snow.

We do not consider the effect of convection processes on heat transport because convective processes depend not only on the conductive properties of the material, but also on its permeability (Sturm and Johnson, 1991; Arakawa et al., 2009; Zermatten et al., 2011).

2 Methods

2.1 Sample preparation

2.1.1 Snow samples

Snow blocks were carefully taken from a natural snowpack. The block was then cut to size for the HFP measurement. In the same block, after the HFP measurements, two horizontal NP measurements were done. This way, an eventual change due to the HFP heating could be checked. Finally, the center of the block used for the HFP measurement was carefully inserted in a sample holder for the micro-computed tomography (μ-CT) measurements (see Sect. 2.3). The inner diameter of the μ-CT sample holder was 36.9 mm. 8 different snow types were analyzed. The snow properties of each sample are summarized in Table 1. All the experiments were conducted within a cold laboratory at a constant temperature of $-20\,^{\circ}$C.

Additional snow samples were used to calculate the anisotropy of the thermal conductivity with the SIM. The properties of these samples are shown in Table 2.

2.1.2 Inert samples for comparison between needle probe and heat flux plate

The results of NP and HFP measurements were compared using several common porous and non-porous materials. Snow thermal conductivity ranges from 0.024 (k_{air}) to $0.8\,\mathrm{W\,m^{-1}\,K^{-1}}$. We selected materials that cover this range, and are suitable for both HFP and NP. We used polystyrene foam, plasticine (Fimo), paraffin wax (Glorex), and water with 5 % agar-agar (Morga AG). Similar materials were used by Pinzer and Schneebeli (2009a). In addition, we used granular and sintered coarse-grained sea salt (grain size $2\,\mathrm{mm} \pm 1\,\mathrm{mm}$) as substitute for snow. These materials do not undergo a phase change at the temperature range of the experiments and give minimal contact resistance for both HFP and NP.

2.2 Measurement of thermal conductivity

2.2.1 Transient measurement with the needle probe

The theory for transient measurements with a NP for an ideally conducting material is well known (Blackwell, 1954; Carslaw and Jaeger, 1959; Hartley and Black, 1976). The method was applied for thermal conductivity measurements in snow by different groups (Sturm and Johnson, 1992; Morin et al., 2010).

The thermal conductivity, k^{NP} ($\mathrm{W\,m^{-1}\,K^{-1}}$), is calculated as

$$k = \frac{q}{4\pi\ \Delta T} \ln \frac{t_2}{t_1}, \tag{1}$$

where t_2 (s) and t_1 (s) are the linear time region of the measurement, q ($\mathrm{W\,m^{-1}}$) the heating power, ΔT (K) the temperature difference. Note that k^{NP} corresponds to k_z in case of an isotropic medium.

In this study, we used an NP (TP02, Hukseflux Thermal Sensors) as used by Morin et al. (2010) and Calonne et al. (2011). The needle is 1.2 mm in diameter and 150 mm long. The applied heating power was $0.07\,\mathrm{W\,m^{-1}}$ in order to have a total temperature increase smaller than 2.5 °C in the snow. This corresponds to a maximal temperature increase of 1 °C in the time interval $t_1 - t_2$ used in Eq. (1). In order to avoid the

Table 1. Structural properties of the snow samples used for the intercomparison of the different measurement methods*.

Grain shape, main class	ISC	Density	SSA	i.th	i.sp
		$\mathrm{kg\,m^{-3}}$	$\mathrm{mm^{-1}}$	mm	mm
Depth Hoar	DHch	172	12.90	0.20 ± 0.07	1.76 ± 1.27
Faceted Crystals	FCso	230	12.71	0.25 ± 0.07	0.42 ± 0.15
Rounded Grains	RGxf	246	17.63	0.17 ± 0.04	0.36 ± 0.14
Faceted Crystals	FCxr	251	17.05	0.18 ± 0.05	0.40 ± 0.14
Rounded Grains	RGsr	253	14.47	0.22 ± 0.05	0.30 ± 0.13
Rounded Grains	RGlr	267	16.16	0.19 ± 0.07	0.41 ± 0.16
Rounded Grains	RGsr	286	8.84	0.34 ± 0.13	0.81 ± 0.36
Rounded Grains	RGsr	331	19.89	0.16 ± 0.03	0.27 ± 0.09

* Snow type: description, ISC: International classification for seasonal snow on the ground (Fierz et al., 2009), Density: gravimetrically determined, SSA: specific surface area from tomography, i.th: thickness of ice structures by tomography, i.sp: pore size by tomography.

Table 2. Structural properties of the additional snow samples used for the simulation of thermal conductivity anisotropy*.

Grain shape, main class	ISC	Density	SSA	i.th	i.sp
		$\mathrm{kg\,m^{-3}}$	$\mathrm{mm^{-1}}$	mm	mm
Precipitation Particles	PPsd	91	64.65	0.05 ± 0.03	0.45 ± 0.19
Rounded Grains	RGsr	118	25.09	0.13 ± 0.04	0.56 ± 0.34
Rounded Grains	RGsr	155	29.03	0.12 ± 0.03	0.31 ± 0.11
Rounded Grains	RGsr	155	27.15	0.12 ± 0.03	0.33 ± 0.12
Rounded Grains	RGsr	164	26.78	0.12 ± 0.03	0.34 ± 0.13
Rounded Grains	RGsr	173	23.41	0.14 ± 0.04	0.36 ± 0.14
Rounded Grains	RGsr	182	25.50	0.13 ± 0.03	0.30 ± 0.11
Rounded Grains	RGsr	191	26.39	0.13 ± 0.03	0.28 ± 0.10
Rounded Grains	RGsr	191	24.90	0.13 ± 0.03	0.32 ± 0.12
Rounded Grains	RGsr	191	31.34	0.10 ± 0.03	0.24 ± 0.09
Rounded Grains	RGsr	200	24.85	0.13 ± 0.04	0.29 ± 0.11
Depth Hoar	DHcp	209	12.28	0.23 ± 0.14	0.93 ± 0.53
Depth Hoar	DHcp	228	11.31	0.25 ± 0.13	0.78 ± 0.37
Depth Hoar	DHcp	237	15.99	0.17 ± 0.07	0.49 ± 0.23
Depth Hoar	DHcp	237	16.37	0.16 ± 0.07	0.47 ± 0.22
Faceted Crystals	FCso	246	11.65	0.26 ± 0.09	0.54 ± 0.21
Depth Hoar	DHcp	246	10.51	0.29 ± 0.20	0.82 ± 0.44
Depth Hoar	DHcp	255	12.97	0.20 ± 0.10	0.62 ± 0.33
Melt Forms	MFcl	264	8.21	0.35 ± 0.13	0.80 ± 0.35
Rounded Grains	RGlr	264	11.89	0.26 ± 0.09	0.49 ± 0.20
Melt Forms	MFcl	273	9.40	0.31 ± 0.12	0.63 ± 0.29
Depth Hoar	DHcp	282	14.05	0.17 ± 0.07	0.54 ± 0.32
Melt Forms	MFcl	282	14.72	0.21 ± 0.06	0.34 ± 0.13
Depth Hoar	DHcp	291	13.51	0.19 ± 0.10	0.51 ± 0.28
Melt Forms	MFcl	300	15.14	0.21 ± 0.06	0.31 ± 0.12
Faceted Crystals	FCso	309	7.11	0.41 ± 0.18	0.71 ± 0.29
Melt Forms	MFcl	364	9.62	0.31 ± 0.11	0.40 ± 0.17

* Snow type: description, ISC: International classification for seasonal snow on the ground (Fierz et al., 2009), Density: gravimetrically determined (correspond to the local density of the computed volumes within 15 %), SSA: specific surface area from tomography, i.th: thickness of ice structures by tomography, i.sp: pore size by tomography.

effect of a high contact resistance, the first 30 s of the measurement were discarded. Convection effects occurred after 100 s. For these reasons, the thermal conductivity was calculated between $t_1 = 30$ s and $t_2 = 100$ s (Morin et al., 2010; Sturm et al., 1997), which corresponds to the linear portion of Eq. (1), when plotting the temperature in function of time on logarithmic scale.

Before use, the accuracy of the NP was checked with measurements in glycerin 80 % (Glycerin CAS 56-81-5).

In a homogenous block of snow (45 cm × 45 cm × 45 cm), with the sides parallel and orthogonal to the layers, two horizontal and two vertical measurements were performed. The needle was inserted such that the temperature sensor of the needle was always positioned at the same height of the block. From these four measurements, k_z, k_x and the anisotropy (α, see Sect. 2.2.2) were calculated.

2.2.2 Anisotropy

Grubbe et al. (1983) analyzed the case of line source measurements in anisotropic rock. He developed the general case, when the bedding plane is inclined to the surface of the Earth. Assuming that NP measurements in snow are always parallel or orthogonal to the layering of the snowpack, the following formulas can be used. If the z-axis of the coordinate system is orthogonal to the snow surface, then $k_x = k_y$ in the horizontal plane and k_z in the vertical plane. If the needle is horizontally inserted, the following components are measured (see also Fig. 1):

$$k_h^{NP} = \sqrt{k_x k_z}, \tag{2}$$

with a vertically inserted needle:

$$k_v^{NP} = \sqrt{k_x^2} \quad \text{for} \quad k_x = k_y. \tag{3}$$

The vertical component k_z can then be extracted from

$$k_z = \frac{k_h^{NP2}}{k_x} = \frac{k_h^{NP2}}{k_v^{NP}}. \tag{4}$$

We define the anisotropy factor $\alpha = k_z/k_x$, which is the inverse of the factor A used by Grubbe et al. (1983) but the same as the anisotropy coefficient used by Calonne et al. (2011). α can be better compared qualitatively by the anisotropy factor γ of Izumi and Huzioka (1975), which is defined as $\gamma = (k_z - k_x)/(k_z + k_x)$.

Therefore, k_z, if the measurement is done with a horizontal NP, is

$$k_z = \sqrt{\alpha} k_h^{NP}. \tag{5}$$

2.2.3 Steady-state measurement with the guarded heat flux plate

The guarded HFP applies a constant heat flux at the bottom of the snow sample. After equilibrium is reached, the heat fluxes at the top and bottom of the sample are equal. The difference between the top and bottom temperatures is measured. As the geometry of the sample is known, the thermal conductivity k^{HFP} (W m^{-1} K^{-1}) is

$$k^{HFP} = q_f h \frac{1}{\Delta T}, \tag{6}$$

where q_f (W m^{-2}) is the heat flux across the sample, h (m) is the height of the sample and ΔT (K) is the temperature difference. In our measurements, the layering was parallel to the plates and therefore $k_z = k^{HFP}$.

In order to avoid heat convection and snow metamorphism, the applied heat flux and the resulting temperature gradient were kept at $\left(\nabla T = \left[10 - 15\,\mathrm{K\,m^{-1}}\right]\right)$ and the temperature at −16 °C.

The design of the HFP is based on the work of Köchle (2009) (Fig. 2). The geometrical design and the main characteristics of the HFP are: (i) the heat flux is constant, (ii) the sample is insulated and guarded such that the heat flow is perpendicular to the plates, (iii) the heat flux sensors are guarded by additional surrounding material of equal conductivity, (iv) the temperature difference is measured as precisely as possible, and (v) the size of the sample chamber must be sufficiently large so that an undisturbed snow sample can be used. We built an apparatus with a plate size of 210 mm × 210 mm and an adjustable height between 5 and 80 mm. The base of the chamber consisted of 30 mm-thick styrofoam insulation. On top of the insulation, a film heater (Minco, Type

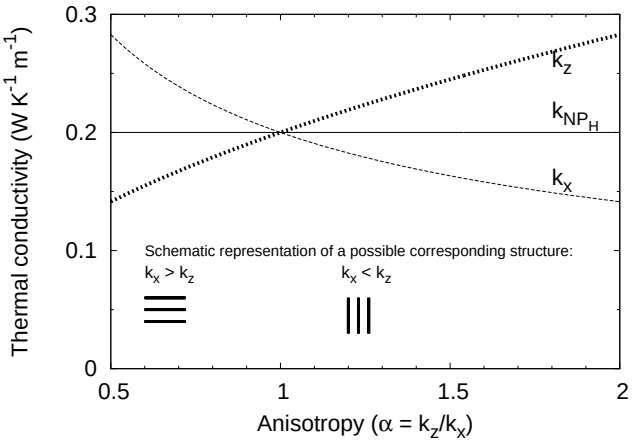

Fig. 1. The effect of anisotropy of snow on the vertical component of thermal conductivity (k_z) if thermal conductivity is measured with a horizontally inserted NP. Calculations are based on Grubbe et al. (1983). The range of the anisotropy factor between 0.5 and 2 is typical for natural snow. The horizontal line at 0.2 W m^{-1} K^{-1} indicates the measured thermal conductivity with the NP horizontally inserted. For an anisotropy factor, $\alpha < 1$, k_z is underestimated by up to 25 %. In case of $\alpha > 1$, k_z is underestimated by up to 25 %. Also shown is the horizontal component of the thermal conductivity, $k_x = k_v^{NP}$, which corresponds to the value measured with a vertically inserted NP.

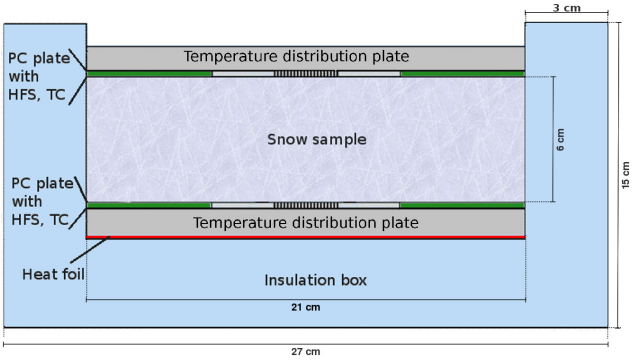

Fig. 2. Design of the HFP (Köchle, 2009). PC: polycarbonate plate, HFS: heat flux sensor, TC: thermocouples. HFS and TC are in the center of the PC plate.

HK5170) was glued to a steel plate (8 mm thick). This plate served to distribute the heat and damped any remaining fluctuations by the inherent heat capacity of steel. A polycarbonate plate (3 mm thick) with a center hole of 100 mm followed. The heat flux sensor (Hukseflux PU_43) was placed in the hole. The sensor had a thickness of 3 mm, and an active sensing area of 30 mm × 30 mm. The total error of the heat flux measurement was $\pm 0.1\,\mathrm{W\,m^{-2}}$ at the typical heat flux of $2\,\mathrm{W\,m^{-2}}$. The outer area served as a thermal shield for the sensor. The polycarbonate plate and the heat flux sensor have the same thermal conductivity of $0.25\,\mathrm{W\,m^{-1}\,K^{-1}}$. The snow sample, usually 60 mm thick, was placed on the polycarbonate plate. The sample was covered again with a heat flux sensor inserted in a polycarbonate plate. A 6 mm thick aluminum plate improved contact further. The polycarbonate plates were covered with a thin layer of thermal grease (Dow Corning 340, $k = 0.55\,\mathrm{W\,m^{-1}\,K^{-1}}$ to reduce the contact resistance between snow and plate. The temperature difference between the plates was measured using two K-type thermocouples in series. The precision of the thermocouples were ±0.03 °C. The absolute temperature was measured at the bottom of the plate using a RTD-sensor (Minco, Type S17621) with an absolute precision of ±0.4 °C. The sides of the apparatus were covered with 30 mm-thick styrofoam insulation. The HFP apparatus was placed in an insulated chamber of 70 cm × 70 cm × 80 cm. This small chamber was heated up to −15 °C in a cold laboratory kept at −20 °C, in order to reduce temperature variations, which affected the stability of the measurements. Data logging was done with a Campbell CR10 data logger.

2.2.4 Latent heat flux

Pinzer and Schneebeli (2009b) and Pinzer (2009) made direct measurements of the recrystallization rate of snow, and by this the effective latent heat flux. They could show that the vapor diffusivity in snow, D_{eff}, is close to the diffusivity in air (Giddings and LaChapelle, 1962; Sokratov and Maeno, 2000).

The latent heat flux is calculated using the effective vapor flux present in the snow sample during a HFP experiment. The vapor flux is defined as

$$J_z = D_{\mathrm{H_2O}} \Delta C_z M_{\mathrm{H_2O}}, \quad \text{with} \quad \Delta C_z = \frac{|e_b - e_t|}{h \kappa_B T_m}, \tag{7}$$

where J_z ($\mathrm{kg\,m^{-2}\,s^{-1}}$) is the heat flux in the z-direction, $D_{\mathrm{H_2O}}$ ($\mathrm{m^2\,s^{-1}}$) is the water vapor diffusivity, ΔC_z ($\mathrm{Pa\,m^{-1}}$) is the gradient of vapor pressure, $M_{\mathrm{H_2O}}$ (kg) is the mass of a water molecule, e_b and e_t (Pa) are the bottom and top pressures according to Murphy and Koop (2005) respectively, h (m) is the height of the sample, κ_B ($\mathrm{J\,K^{-1}}$) is the Boltzmann constant and T_m (K) is the mean temperature of the sample.

The latent heat flux is then defined as

$$q_L = J_z L \quad \text{and} \quad q_t = q_f + q_L, \tag{8}$$

where q_L ($\mathrm{W\,m^{-2}}$) is the latent heat flux, L ($\mathrm{J\,kg^{-1}}$) is the latent heat of sublimation of ice. q_t ($\mathrm{W\,m^{-2}}$) is the measured heat flow, which includes both the sensible (q_f) and the latent (q_L) heat fluxes.

The values used for these equations and the calculation of the latent heat flux are in Appendix A.

2.3 Tomography and direct numerical simulation

Each sample was directly measured, without further preparation, in the μ-CT (Scanco micro-CT80). The temperature during a measurement was controlled and kept at a constant temperature of −15 °C. The nominal resolution of the images was 18 µm. The size of the original image was 2048 × 2048 × 416 voxels, the scanned volume had a diameter of 36 mm and a height of 7.5 mm.

2.3.1 Image processing

From the μ-CT measurements, a volume of 400 × 400 × 400 voxels (7.2 mm × 7.2 mm × 7.2 mm) was extracted from the original data. This volume was then segmented to a binary image. A Gauss filter ($\sigma = 1$, support = 2) was applied, then the ice structure was segmented using an adaptive threshold. The obtained density of the ice volume was compared to the measured density of the snow sample in order to control for the segmentation procedure. If the difference in density was higher than 12 %, the threshold in the segmentation process was manually corrected to obtain the right density within 12 %. Depth hoar samples were up-scaled to a nominal resolution of 36 µm. This was necessary to conduct the SIM within a reasonable time and with a larger representative elementary volume (REV) of a sufficient size (volume of 10.8 mm × 10.8 mm × 10.8 mm. From each sample, except depth hoar, two sub-samples where taken to estimate intra-sample variability.

2.3.2 Direct numerical simulation

The numerical simulation uses the code described Kaempfer and Plapp (2009) and Pinzer (2009). It is a linear steady-state thermal finite element simulation. The finite element mesh consists of hexahedral elements, which correspond to the voxels of the μ-CT measurements. As an input the simulation requires the temperature gradient in the snow and the thermal conductivity of air and ice. The boundary conditions are constant top and bottom temperatures and insulated sidewalls. No phase change is implemented in the model.

We used the following values: $\nabla T = 50\,\mathrm{K\,m^{-1}}$, $k_{\mathrm{ice}} = 2.34\,\mathrm{W\,m^{-1}\,K^{-1}}$ (k_{ice} at $-20\,^{\circ}\mathrm{C}$, Slack, 1980) and $k_{\mathrm{air}} = 0.024\,\mathrm{W\,m^{-1}\,K^{-1}}$. Based on the simulated heat flux and the prescribed temperature gradient the thermal conductivity is calculated as

$$k_{\mathrm{x,z}}^{\mathrm{SIM}} = q_{\mathrm{x,z}}/\nabla T. \quad (9)$$

For each k_{z} and k_{x} an independent simulation is necessary.

3 Results

3.1 Calibration of the needle probe and the heat flux plate

We measured the thermal conductivity of the inert materials (polystyrene foam, plasticine, wax at room temperature and at cold lab temperature ($-20\,^{\circ}\mathrm{C}$), agar gel (5 %), and salt in granular form and as a sintered block) with the NP and the HFP (Fig. 3). In homogenous, isotropic and non-porous materials (plasticine, polystyrene, wax), k^{NP} and k^{HFP} were similar. k^{NP} was slightly higher than k^{HFP} for agar, but k^{NP} was 30–40 % lower than k^{HFP} for the granular salt. Similarly, a long heating time (100 s) resulted in a 15 % lower k^{NP} than k^{HFP} for the sintered salt block. A short heating time (30 s) resulted in a k^{NP} 70 % lower than the two other measurements.

A linear regression was calculated for the short and the long heating time NP versus HFP, forcing the curve through the origin. The measurement of the salt block at short heating time was not considered. The correlation between NP measurements and HFP measurements was high: we found that the regression equation for both the short and long heating time was $k^{\mathrm{NP}} = 0.96k^{\mathrm{HFP}}$ with a root mean square error of 0.07, and all points within 99 % significance.

3.2 Numerical simulation

The thermal conductivity was calculated for all samples listed in Table 1 (all measured and calculated thermal conductivities are listed in the supplementary material). Two independent volumes of each sample were calculated, except for the depth hoar sample, where the size of the REV was too large to extract two independent volumes from the scanned

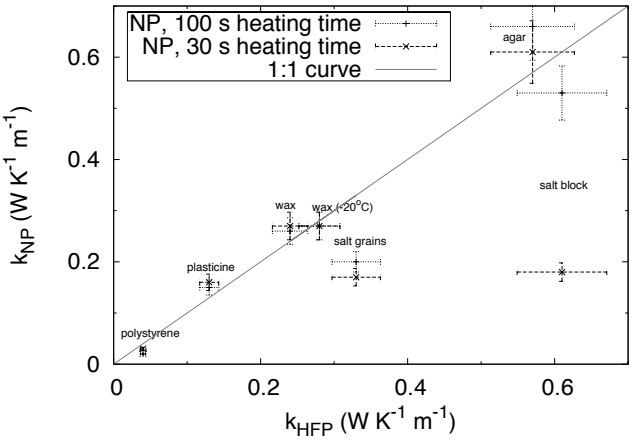

Fig. 3. Thermal conductivity of several inert, isotropic materials measured with the heat flux plate (HFP) and the needle probe (NP). HFP and NP have similar values for inert, non-porous materials. Measurements with NP in agar are known to be too high due to convection (Boumaza and Redgrove, 2003). The NP measures a too low a value compared to the HFP for the porous materials (granular salt grains and sintered sea salt). The k^{NP} resulting from a 100 s instead of a 30 s measurement increases thermal conductivity almost threefold for the sintered salt block.

volume. Density and thermal conductivity of these samples are shown in Supplementary Table 1. The density of the two paired samples varied between 0.1 % and 3.2 %, (average 1.3 %), the thermal conductivity between 0.5 % and 34 % (average 6.1 %). The outlier with 34 % was for the faceted snow with a density of $261\,\mathrm{kg\,m^{-3}}$.

The result of the simulation depends on the threshold for the segmentation of the ice structure. To test for the sensitivity, we increased the threshold by 10 % for one sample. This increased the volumetric density by 4 % and the thermal conductivity by 8 %.

3.3 Comparison of the needle probe and direct numerical simulation

The vertical and horizontal thermal conductivities measured with long heating-time NP, corrected for anisotropy, were systematically lower by 10–35 % compared to the values calculated by the SIM (Fig. 4). We found that the trend in anisotropy is in most cases the same ($k_{\mathrm{x}}^{\mathrm{SIM}} > k_{\mathrm{z}}^{\mathrm{SIM}}$ if $k_{\mathrm{x}}^{\mathrm{NP}} > k_{\mathrm{z}}^{\mathrm{NP}}$). The correlation between k^{SIM} and k^{NP} was $k^{\mathrm{NP}} = 0.79k^{\mathrm{SIM}} - 0.021$ (root mean square error 0.023). The difference between the null hypothesis (the 1 : 1 line) and the correlation was significant at the 99 % level.

3.4 Comparison of the three methods

The vertical component k_{z} measured by the NP were in all samples lower than the ones measured by HFP and calculated by SIM (Fig. 5). $k_{\mathrm{z}}^{\mathrm{SIM}}$ are 3 % to 25 % lower (average 20 %) than $k_{\mathrm{z}}^{\mathrm{HFP}}$ and $k_{\mathrm{z}}^{\mathrm{NP}}$ are 15 % to 55 % lower (average 35 %)

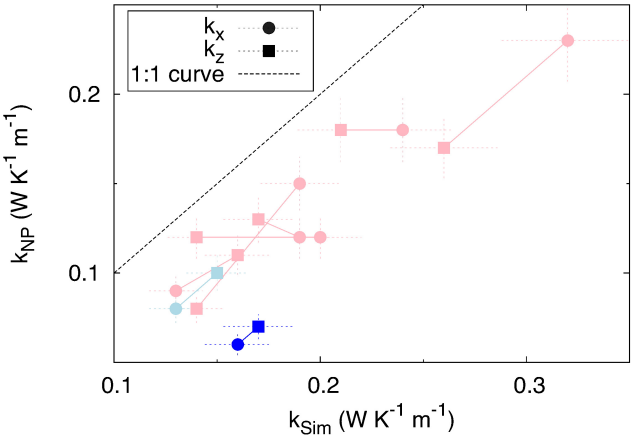

Fig. 4. Comparison of the horizontal and vertical component of the thermal conductivity from direct numerical simulation, k^{SIM} and needle probe measurement, k^{NP}. All measurements, except two, show the same trend in anisotropy, however all components of $k^{\mathrm{NP}}_{\mathrm{x,z}}$ are systematically lower than $k^{\mathrm{SIM}}_{\mathrm{x,z}}$. Colors correspond to the International classification for seasonal snow on the ground (Fierz et al., 2009). Light pink: rounded grains, light blue: faceted crystals, blue: depth hoar.

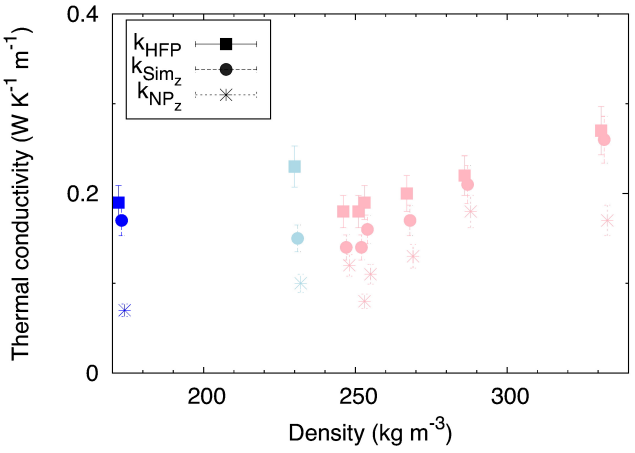

Fig. 5. Comparison of the vertical components of the thermal conductivity, k_{z} for the three methods. HFP gave always the highest value and the NP the lowest one, the SIM is close to HFP. The bars indicate estimated error. Colors correspond to the International classification for seasonal snow on the ground (Fierz et al., 2009). Light pink: rounded grains, light blue: faceted crystals, blue: depth hoar.

than $k^{\mathrm{HFP}}_{\mathrm{z}}$ (Fig. 6). The differences between NP compared to SIM and HFP were highly significant, and the difference between SIM and HFP was significant.

The comparison of the relative change of $k^{\mathrm{NP}}_{\mathrm{h}}$ between the two NP measurements before and after the HFP measurements showed a mean increase of $6.3\,\% \pm 8.4\,\%$ (minimum $-4.9\,\%$, maximum $+18.5\,\%$).

3.5 Comparison of thermal conductivity with previous studies

The effective thermal conductivities, calculated by the SIM ($k_{\mathrm{eff}} = (k_{\mathrm{z}} + k_{\mathrm{x}})/2$), corresponds well to the data set and the fitting equation presented in Calonne et al. (2011) (Fig. 7). However, the snow samples of Calonne et al. (2011) all have a relatively small anisotropy, except for four samples that are either faceted snow or depth hoar. By taking into account only depth hoar (DH) and faceted crystals (FC) samples, which both have a higher conductivity in the vertical direction, it appears that the effective thermal conductivity of these samples is much more different from k_{z} than for the other samples, such as small rounded grains. By fitting k_{z} of depth hoar and facets samples, the following regression equation is obtained:

$$k_{\mathrm{z}} = 3 \times 10^{-6}\rho^2 - 1.06 \times 10^{-5}\rho + 0.024, \qquad (10)$$

with a correlation coefficient of 0.986 (for 17 samples, 13 samples from this study and 4 from the study of Calonne et al., 2011) and with k_{z} corresponding to the thermal conductivity of air when snow density is zero, as suggested in Calonne et al. (2011) (Fig. 7).

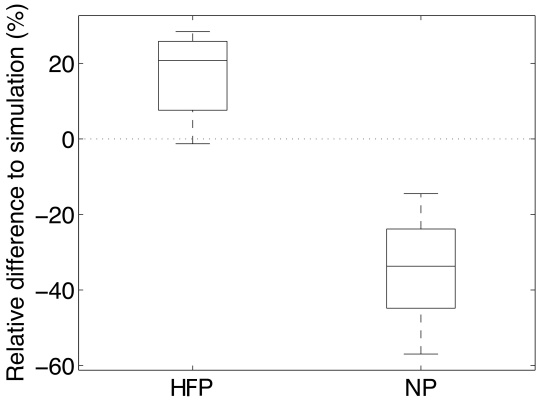

Fig. 6. Relative differences of k_{z} for the 8 samples used for both HFP and NP with SIM as reference. HFP values are 20 % higher, NP values are 35 % lower than those obtained by SIM. The median of the relative differences is the line inside the box; the top and the bottom of the boxes are the quartiles.

3.6 Anisotropy factor

$k^{\mathrm{SIM}}_{\mathrm{z,y}}$ was calculated for 35 samples in total (Fig. 8). The temperature of ice and air was always set to $-20\,^{\circ}\mathrm{C}$. We found that the majority of samples showed a certain degree of anisotropy, and isotropic snow seemed to be rather the exception than the rule. The anisotropy factor α was calculated from the data of Izumi and Huzioka (1975) for comparison. The anisotropy of our snow samples with a similar snow structure and density showed approximately the same anisotropy values as those of Izumi and Huzioka (1975). The anisotropy factor was also compared to Calonne et al. (2011). All the data are consistent: depth hoar samples and facets

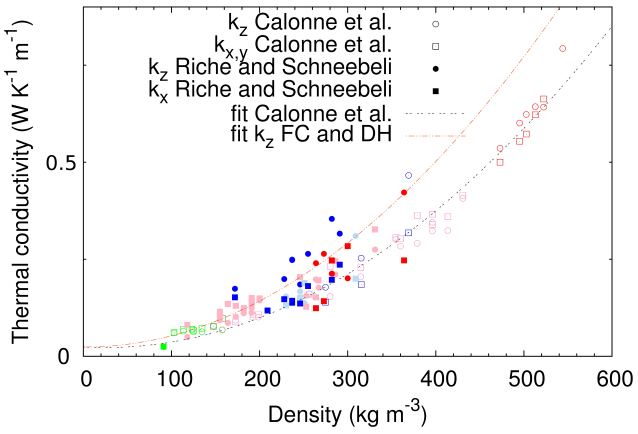

Fig. 7. Thermal conductivities as a function of snow density. Comparison to the data of Calonne et al. (2011). Colors and abbreviations correspond to the International classification for seasonal snow on the ground (Fierz et al., 2009). Lime: precipitation particles (PP), forest green: decomposing and fragmented precipitation particles (DF), light pink: rounded grains (RG), light blue: faceted crystals (FC), blue: depth hoar (DH), red: melt forms (MF).

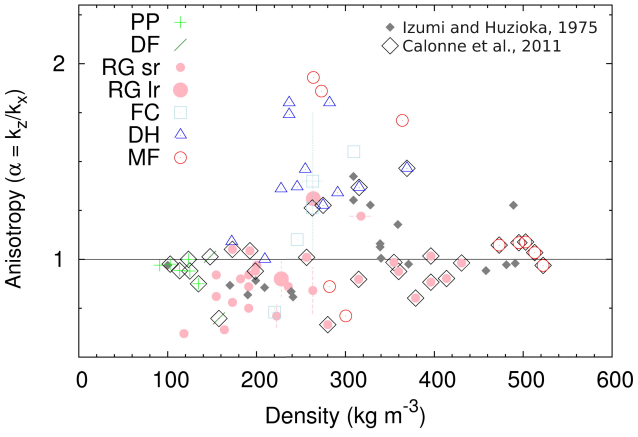

Fig. 8. Anisotropy factor α of different snow types as a function of density (local density of the volume used to compute the thermal conductivity). The anisotropy shown here was calculated from SIM. The 8 samples measured with SIM, HFP and NP are indicated with error bars. Colors, shapes and abbreviations correspond to the International classification for seasonal snow on the ground (Fierz et al., 2009). Lime: precipitation particles (PP), forest green: decomposing and fragmented precipitation particles (DF), light pink: rounded grains (RG, small rounded particles: RGsr, large rounded particles: RGlr), light blue: faceted crystals (FC), blue: depth hoar (DH), red: melt forms (MF).

conduct heat better in the vertical direction. Rounded grains are almost isotropic or conduct heat better in the horizontal direction (Fig. 8).

3.7 Latent heat flux in the heat flux plate

All HFP measurements were carried out at a temperature of $-16\,^{\circ}\mathrm{C} \pm 1\,^{\circ}\mathrm{C}$. For a temperature gradient of $11\,\mathrm{K\,m^{-1}}$, the calculated latent heat flux was $0.01\,\mathrm{W\,m^{-2}}$. In the HFP measurement, the measured heat flux was approximately $2\,\mathrm{W\,m^{-2}}$, therefore the latent heat flux (calculated) represented less than 1 % of the measured heat flux (Eq. 8). The latent heat flux had therefore no significant effect on the heat flux at this temperature. However, at higher temperatures, latent heat flux becomes significant. At a temperature of $-5\,^{\circ}\mathrm{C}$ and with the same temperature gradient, the latent heat flux would increase to $0.14\,\mathrm{W\,m^{-2}}$, corresponding to a contribution of 14 %.

4 Discussion

The thermal conductivities of NP and HFP in the inert, isotropic and solid reference materials lie almost perfectly on the 1 : 1 line (Fig. 3). Both methods, NP and HFP, gave the same absolute values of thermal conductivity in these materials. Both instruments showed no temperature dependence, tested with wax at 20 °C and −20 °C. The higher k^{NP} with agar was caused by convection, and it was also observed by Boumaza and Redgrove (2003). The NP measurement in sintered salt with a short heating time (30 s) is a reminder that NPs with short heating time do not correctly measure thermal conductivity due to contact resistance problems present in porous materials (Riche and Schneebeli, 2010a). The long heating time NP measurements in granular and sintered salt resulted in significantly lower values (50 % for granular, and 20 % for sintered salt grains respectively) than the HFP measurements. We think that there are two possible reasons. The first is that the high contact resistance influenced linearity within the evaluated time span. However, a longer measurement time (longer than 100 s) was not possible, because of the clearly visible onset of convective processes (Sturm and Johnson, 1992). The second reason can be the heterogeneity of the temperature field, as already pointed out in Calonne et al. (2011). It is well known from the measurement of the dielectric properties that the radius of curvature of the electrode must be much larger than the snow grain diameter (Mätzler, 1996). The size of the salt grains was about twice the size of the diameter of the NP, so this empirical rule was clearly violated.

The HFP always gave values higher than the SIM and the NP (Fig. 5). The difference between HFP and SIM can mainly be explained by the sensitivity of the SIM to the small variations of snow density. It happened that the densities of the μ-CT-measurements were lower than the measured density of the snow. This effect will cause simulated values lower than the real thermal conductivity value. HFP methods are considered less reliable than NP, because they are more susceptible to measurement-induced metamorphism (Sturm and

Johnson, 1992). We observed such a predicted increase of k on the order of 5 % (see Sect. 3.4). However, this increase did not explain the much larger difference between NP compared to SIM and HFP.

The difference between HFP and SIM could be caused by two factors. The thermal grease applied could increase the thermal conductivity. Therefore a correction in the effective height would be necessary. A 2 mm thick layer of thermal grease on both plates would lead to an increase of about 5 % in k^{HFP}. Such a correction was not applied. Another reason could be that the finite resolution of the μ-CT and the threshold eliminated heat-conducting bonds. This leads to a maximal absolute uncertainty of k^{SIM} by 10–15 %.

k^{NP} compared to k^{SIM} gave consistent results. They show the same anisotropy trend in most of the measurements (Fig. 4). However, k^{NP} corrected for anisotropy was significantly lower than k^{SIM} and k^{HFP}. Riche and Schneebeli (2010a) showed that significant microstructural changes around the needle occur, but suggested that this effect was only important for short heating times. Measurements in glycerin show no effect of an air gap on the thermal conductivity (M. Sturm and J. B. Johnson, personal communication, 2010). Calonne et al. (2011) suggested that the measured volume around the NP is too small. Another explanation could be that the thermal field is too far from homogenous conditions for such a thin NP to apply the theory developed for transient methods (Blackwell, 1954; Mätzler, 1996).

The thermal conductivity values obtained with SIM correspond well to other studies (shown in Fig. 7). A regression equation was calculated for k_{z} for depth hoar and faceted crystals samples. This fit shows that the anisotropy of the snow samples has to be taken into account. Thermal conductivity components depend not only on the density but also on the snow type. It is therefore difficult to give only one empirical relation between thermal conductivity and structural properties (such as density) that would be correct for all snow samples.

Izumi and Huzioka (1975) and Yamada et al. (1974) showed the existence of anisotropic thermal conductivity in snow. We found that a considerable anisotropy exists for most snow types. The single new snow sample that we measured was almost isotropic. Snow samples with small rounded grains had an $\alpha < 1$, and faceted snow and depth hoar had in general $\alpha > 1$, which is similar to the results of Izumi and Huzioka (1975) and Calonne et al. (2011). All depth hoar samples with a density above 200 kg m^{-3} had an α between 1.25 and 1.75. Melt forms covered a very broad range of α between 0.75 and 1.75, probably depending on the anisotropy before wet snow metamorphism started. Our measurements corroborate that $k_{\mathrm{h}}^{\mathrm{NP}}$ must be corrected by Eq. (5) to give a correct k_{z}. This correction, as proposed by Grubbe et al. (1983), clearly reduced the difference between NP and SIM. The most comprehensive data sets of thermal conductivity (Sturm et al., 1997, 2002; Sturm and Johnson, 1992) and their fitting equations should be corrected for anisotropy, depending on grain type and density. Such a correction is also necessary in homogenous layers of certain snow types, and should be done in future measurements, especially for long-term measurements with needle-probes (Morin et al., 2010). However, NP still shows a systematic bias to SIM and HFP, even after correction for anisotropy.

Snow pack models are currently one-dimensional (Etchevers et al., 2004). They use a single thermal conductivity component, k_{z}. Anisotropy of snow thermal conductivity could therefore have important consequences for heat flow and energy balance in complex terrain.

Based on the results of Sokratov and Maeno (2000) and Pinzer (2009), the latent heat flux was estimated within a factor of two by Pinzer et al. (2012). So far, the latent heat flux was considered as the major weak point of the HFP. However, at low temperatures (as used in this study), the calculated latent heat flux is less than 1 %; it is therefore negligible. The higher thermal conductivity of the HFP measurements compared to SIM can not be explained on this ground. The thermal grease applied between the plates could cause about 5 % increase, but does not explain completely the difference between the measured values of HFP and SIM.

5 Conclusions

We compared three different methods to measure the thermal conductivity of snow using identical snow samples. This study analyzed the systematic differences found between methods. HFP gave consistently higher results compared to SIM. The NP systematically underestimated the thermal conductivity of snow, even after correction for anisotropy.

We confirm that many snow types are anisotropic regarding thermal conductivity. This implies that at least one horizontal and one vertical measurement with the NP is required, and the individual layers must be sufficiently (at least a few cm) thick. Natural anisotropy can cause an variation of ± 25 %. We also found that anisotropy is not always correlated with grain shape (Fig. 8). However, the scatter is very large, and a correction for anisotropy is difficult.

We found that the reproducibility of all methods was similar, with relative differences between the methods of about ± 10 %. The HFP proved to be reliable. HFP are very time-consuming, and best suited for laboratory experiments. In combination with SIM, it could also be used to investigate the effect of latent heat flux on the microstructure.

The current design of the NP produces two problems for snow thermal conductivity measurements. The first is systematically too low a value of the measured thermal conductivity, and the second is that at least two measurements are necessary to determine the anisotropy of the thermal conductivity. HFP and SIM gave similar results. However, HFP is a very time-consuming method and measures only k_{z}. Direct numerical simulations seems to be the most precise method to obtain reliable values of the effective thermal conductivity

of snow. Recent improvements in imaging the microstructure of snow and modeling porous structures make this method widely available.

Appendix A

Calculation of the latent heat flux

The relevant constants for the calculation of the latent heat flux in snow are: Avogadro number: $N_a = 6.022 \times 10^{23}$ [particles per mole], mass of a water molecule: $M_{H_2O} = 18.016 \times 10^{-3}/N_a$ [kg], Boltzmann constant: $k_B = 1.38065 \times 10^{-23}$ [$J K^{-1}$], water diffusivity: $D_{H_2O} = 2.178 \times 10^{-5} \times (1013/840.0) \cdot ((T_{mean} + 273.15)/273.15)^{1.81}$ [$m^2 s^{-1}$], latent heat of ice: 3.34×10^5 [$J kg^{-1}$].

The vapor flux in our experiments was calculated as follows: the mean temperature was $T_{mean} = 257$ K, the bottom temperature was $T_{bot} = 257.25$ K, the top temperature was $T_{top} = 256.75$ K, and the height of the snow sample was $h = 4.5 \times 10^{-2}$ m.

The top and bottom pressure were calculated according to Murphy and Koop (2005):
bottom pressure:
$e_b = e^{(9.55 - 5723.265/T_{bot} + 3.53068 \cdot \log(T_{bot}) - 0.00728332 \cdot T_{bot})}$,
top pressure:
$e_t = e^{(9.55 - 5723.265/T_{top} + 3.53068 \cdot \log(T_{top}) - 0.00728332 \cdot T_{top})}$.

By applying Eq. (7), we obtained $J_z = 3.088 \times 10^{-8}$ kg m^{-2} s^{-1} and from Eq. (8): $q_L = 0.0103$ W m^{-2}.

Supplementary material related to this article is available online at: http://www.the-cryosphere.net/7/217/2013/tc-7-217-2013-supplement.pdf.

Acknowledgements. This work is supported by the Swiss National Science Foundation. The authors thank B. Köchle for the HFP snow measurements, and M. Sturm and J. B. Johnson for the needle probe and discussions, C. Mätzler for bringing up the idea of the heterogeneity of the temperature field. The authors would also like to thank S. Morin (CNRM-GAME/CEN) and an anonymous reviewer for their comments and suggestions during the review process.

Edited by: D. Riseborough

References

Abels, G.: Beobachtungen der täglichen Periode der Temperatur im Schnee und Bestimmung des Wärmeleitungsvermögens des Schnees als Function seiner Dichtigkeit, Kaiserl. Akad. Wissensch., Rep. Meteorologie, 16, 1–53, 1892 (in German).

Abu-Hamdeh, N. and Reeder, R.: Soil thermal conductivity: Effects of density, moisture, salt concentration, and organic matter, Soil Sci. Soc. Am. J., 64, 1285–1290, 2000.

Ams, C. H., Knackstedt, M. A., Pinczewski, W. V., and Lindquist, W. B.: Accurate estimation of transport properties form microtomographic images, Geophys. Res. Lett., 28, 3361–3364, 2001.

Arakawa, H., Izumi, K., Kawashima, K., and Kawamura, T.: Study on quantitative classification of seasonal snow using specific surface area and intrinsic permeability, Cold Reg. Sci. Technol., 59, 163–168, doi:10.1016/j.coldregions.2009.07.004, 2009.

Armstrong, R. L. and Brun, E.: Snow and Climate, Physical Porcesses, Surface Energy Exchange and Modeliing, Chapter 4.4, Cambridge University Press, 2008.

Arons, E. M. and Colbeck, S. C.: Geometry of heat and mass transfer in dry snow: a review of theory and experiment, Rev. Geophys., 33, 463–493, doi:10.1029/95RG02073, 1995.

ASTM: Test method for steady-state heat flux measurements and thermal transmission properties by means of the guarded-hot-plate apparatus, in: Annual Book of ASTM Standards, vol. C177, doi:10.1520/C0177-04, 2008.

Blackwell, J. H.: A transient-flow method for determination of thermal constants of insulating materials in bulk .1. Theory, J. Appl. Phys., 25, 137–144, 1954.

Boumaza, T. and Redgrove, J.: Use of the transient plane source technique for rapid multiple thermal property measurements, Int. J. Thermophys., 24, 501–512, 2003.

Brandt, R. E. and Warren, S. G.: Temperature measurements and heat transfer in near-surface snow at the South Pole, J. Glaciol., 43, 339–351, 1997.

Brigaud, F. and Vasseur, G.: Mineralogy, porosity and fluid control on thermal-conductivity of sedimentary-rocks, Geophys. J. Int., 98, 525–542, 1989.

Calonne, N., Flin, F., Morin, S., Lesaffre, B., du Roscoat, S. R., and Geindreau, C.: Numerical and experimental investigations of the effective thermal conductivity of snow, Geophys. Res. Lett., 38, L23501, doi:10.1029/2011GL049234, 2011.

Carslaw, H. S. and Jaeger, J. C.: Conduction of heat in solids, 2nd Edn., Clarendon Press, 1959.

Cogne, C.: Experimental data and modelling of thermal properties of ice creams, J. Food Eng., 58, 331–341, doi:10.1016/S0260-8774(02)00396-5, 2003.

Cook, B. I., Bonan, G. B., Levis, S., and Epstein, H. E.: The thermoinsulation effect of snow cover within a climate model, Clim. Dynam., 31, 107–124, doi:10.1007/s00382-007-0341-y, 2007.

De Vries, D.: A nonstationary method for determining thermal conductivity of soil in situ, Soil Sci., 73, 83–89, 1952.

Etchevers, P., Martin, E., Brown, R., Fierz, C., Lejeune, Y., Bazile, E., Boone, A., Dai, Y.-J., Essery, R., Fernandez, A., Gusev, Y., Jordan, R., Koren, V., Kowalczyk, E., Nasonova, N. O., Pyles, R. D., Schlosser, A., Shmakin, A. B., Smirnova, T. G., Strasser, U., Verseghy, D., Yamazaki, T., and Yang, Z.-L.: Validation of the energy budget of an alpine snowpack simulated by several snow models (SnowMIP project), Ann. Glaciol., 38, 150–158, doi:10.3189/172756404781814825, 2004.

Fierz, C., Armstrong, R., Durand, Y., Etchevers, P., Greene, E., McClung, D., Nishimura, K., Satyawali, P., and Sokratov, S.: The International Classification for Seasonal Snow on the Ground, vol. IHP-VII Technical Documents in Hydrology No. 83, UNESCO/IHP, 2009.

Giddings, J. C. and LaChapelle, E.: The formation rate of depth hoar, J. Geophys. Res., 67, 2377–2383, doi:10.1029/JZ067i006p02377, 1962.

Grubbe, K., Haenel, R., and Zoth, G.: Determination of the vertical component of thermal conductivity by line source methods, Zbl. Geol. Palaont. Teil, 1, 49–56, 1983.

Hartley, J. G. and Black, W. Z.: Minimization of measurement errors involved in probe method of determining soil thermal-conductivity, J. Heat Trans.-T. ASME, 98, 530–531, 1976.

Incropera, F. P., Dewitt, D. P., Bergman, T. L., and Lavine, A. S.: Fundamentals of Heat and Mass Transfer, 6th Edn., Wiley, 2006.

Izumi, K. and Huzioka, T.: Studies of metamorphism and thermal conductivity of snow. I, Low Temp. Sci., Ser. A, 33, 91–102, 1975.

Kaempfer, T. and Plapp, M.: Phase-field modeling of dry snow metamorphism, Phys. Rev. E, 79, 17 pp., doi:10.1103/PhysRevE.79.031502, 2009.

Kaempfer, T. U., Schneebeli, M., and Sokratov, S. A.: A microstructural approach to model heat transfer in snow, Geophys. Res. Lett., 32, L21503, doi:10.1029/2005gl023873, 2005.

Köchle, B.: Thermal conductivity of snow, M.S. thesis, Karl-Franzens Universität Graz, 2009.

Lange, M. A.: Measurements of thermal parameters in antarctic snow and firn, Ann. Glaciol., 6, 100–104, 1985.

Mätzler, C.: Microwave permittivity of dry snow, IEEE T. Geosci. Remote, 34, 573–581, doi:10.1109/36.485133, 1996.

Morin, S., Domine, F., Arnaud, L., and Picard, G.: In-situ monitoring of the time evolution of the effective thermal conductivity of snow, Cold Reg. Sci. Technol., 64, 73–80, doi:10.1016/j.coldregions.2010.02.008, 2010.

Murphy, D. M. and Koop, T.: Review of the vapour pressures of ice and supercooled water for atmospheric applications, Q. J. Roy. Meteor. Soc., 131, 1539–1565, doi:10.1256/Qj.04.94, 2005.

Nesvadba, P.: Methods for the measurement of thermal conductivity and diffusivity of foodstuffs, J. Food Eng., 1, 93–113, 1982.

Petrasch, J., Schrader, B., Wyss, P., and Steinfeld, A.: Tomography-Based Determination of the Effective Thermal Conductivity of Fluid-Saturated Reticulate Porous Ceramics, J. Heat Transf., 130, 032602, doi:10.1115/1.2804932, 2008.

Pinzer, B.: Dynamics of Temperature Gradient Snow Metamorphism, Ph.D. thesis, ETH Zurich Nr. 18456, 2009.

Pinzer, B. and Schneebeli, M.: Breeding snow: an instrumented sample holder for simultaneous tomographic and thermal studies, Meas. Sci. Technol., 20, 095705, doi:10.1088/0957-0233/20/9/095705, 2009a.

Pinzer, B. R. and Schneebeli, M.: Snow metamorphism under alternating temperature gradients: Morphology and recrystallization in surface snow, Geophys. Res. Lett., 36, L23503, doi:10.1029/2009GL039618, 2009b.

Pinzer, B. R., Schneebeli, M., and Kaempfer, T. U.: Vapor flux and recrystallization during dry snow metamorphism under a steady temperature gradient as observed by time-lapse micro-tomography, The Cryosphere, 6, 1141–1155, doi:10.5194/tc-6-1141-2012, 2012.

Popov, Y. A., Pribnow, D. F. C., Sass, J. H., Williams, C. F., and Burkhardt, H.: Characterization of rock thermal conductivity by high-resolution optical scanning, Geothermics, 28, 253–276, doi:10.1016/S0375-6505(99)00007-3, 1999.

Pribnow, D. F. C., Davis, E. E., and Fisher, A. T.: Borehole heat flow along the eastern flank of the Juan de Fuca Ridge, including effects of anisotropy and temperature dependence of sediment thermal conductivity, J. Geophys. Res.-Sol. Ea., 105, 13449–13456, 2000.

Riche, F. and Schneebeli, M.: Microstructural change around a needle probe to measure thermal conductivity of snow, J. Glaciol., 56, 871–876, doi:10.3189/002214310794457164, 2010a.

Riche, F. and Schneebeli, M.: Anisotropy evolution of thermal conductivity in natural snow evaluated with X-ray tomography and computer simulations, AGU, Fall Meeting Abstracts, p. A511, 2010b.

Shertzer, R. H. and Adams, E. E.: Anisotropic Thermal Conductivity Model for Dry Snow, Cold Reg. Sci.Technol., 69, 122–128, doi:10.1016/j.coldregions.2011.09.005, 2011.

Slack, G.: Thermal conductivity of ice, Phys. Rev. B, 22, 3065–3071, 1980.

Sokratov, S. A. and Maeno, N.: Effective water vapor diffusion coefficient of snow under a temperature gradient, Water Resour. Res., 36, 1269–1276, doi:10.1029/2000WR900014, 2000.

Sturm, M. and Johnson, J. B.: Natural convection in the subarctic snow cover, J. Geophys. Res., 96, 11657–11671, doi:10.1029/91JB00895, 1991.

Sturm, M. and Johnson, J. B.: Thermal conductivity measurements of depth hoar, J. Geophys. Res., 97, 2129–2139, doi:10.1029/91JB02685, 1992.

Sturm, M., Holmgren, J., König, M., and Morris, K.: The thermal conductivity of seasonal snow, J. Glaciol., 43, 26–41, 1997.

Sturm, M., Perovich, D. K., and Holmgren, J.: Thermal conductivity and heat transfer through the snow on the ice of the Beaufort Sea, J. Geophys. Res.-Oceans, 107, 8043, doi:10.1029/2000JC000409, 2002.

Vonherzen, R. and Maxwell, A. E.: The measurement of thermal conductivity of deep-sea sediments by a needle-probe method, J. Geophys. Res., 64, 1551–1563, 1959.

Yamada, T., Hasemi, T., Izumi, K., and Sato, A.: On the dependencies of the velocities of P-and S-waves and thermal conductivity of snow upon the texture of snow, Low Temp. Sci., Ser. A, 32, 71–80, 1974.

Zermatten, E., Haussener, S., Schneebeli, M., and Steinfeld, A.: Instruments and Methods Tomography-based determination of permeability and Dupuit Forchheimer coefficient of characteristic snow samples, J. Glaciol., 57, 811–816, 2011.